Laser & Photonics Reviews

LASER & PHOTONICS REVIEWS

www.lpr-journal.org

RESEARCH ARTICLE OPEN ACCESS

Pancharatnam–Berry Phase Driven by Electrical Restructuring of Liquid Crystal Polarization Grating Period

Elena Melnikova[1] | Katsiaryna Pantsialeyeva[1] | Alexei Tolstik[1] | Veranika Stanevich[2] | Daminika Dashkevich (Chepeleva)[2] | Anatoli Murauski[2] | Alexander Muravsky[3] | Alina Karabchevsky[4,5]

[1]Department of Laser Physics and Spectroscopy, Belarusian State University, Minsk, Belarus | [2]MTLCD lab, Institute of Chemistry of New Materials of the National Academy of Sciences, Minsk, Belarus | [3]SAL/MTLCD lab, Ecole Paysanne de Lignerolles, Le Thieulin, France | [4]School of Electrical and Computer Engineering, Ben-Gurion University of the Negev, Beer-Sheva, Israel | [5]Department of Physics, Lancaster University, Lancaster, UK

Correspondence: Alina Karabchevsky (alinak@bgu.ac.il)

Received: 6 November 2025 | **Revised:** 18 May 2026 | **Accepted:** 27 May 2026

Keywords: diffraction | geometric phase | liquid crystals | Pancharatnam–Berry phase | phase profile | photoalignment | polarization holography

ABSTRACT

The ability to dynamically reconfigure photonic components is a cornerstone of next-generation optical systems. Nematic liquid crystal materials enable scalable, polarization-sensitive photonic devices for tunable, multifunctional optical platforms. An experimental and theoretical analysis of the diffraction properties of an electrically controlled polarization liquid crystal twist grating is presented here, based on the optical functional concept of the element as a combination of a retarder that provides an optical phase shift and a rotator that determines the polarization plane rotation. Here, we show that, within the operating voltage range corresponding to Mauguin condition violation, the electro–optical response of our electro–optical system is governed by two independent electrically controlled liquid crystal sublayers located within the element. This causes the ambiguity of the element diffraction properties with respect to the side of the radiation input into it. The electrical switching of the diffraction structure period from $\Lambda_1 = 20$ μm to $\Lambda_2 = 10$ μm (the liquid crystal layer thickness is 10 μm) is demonstrated. The device diffraction efficiency reaches 91% at a control voltage of 2.8 V. The possibility of precise electrical control of the device polarization-dependent diffraction properties makes it possible to simultaneously form two circularly polarized orthogonal coherent waves and control their intensity, which is a promising task for modern communications, lidar systems, holographic technologies, quantum computing and information processing.

1 | Introduction

Modern optical technologies are undergoing a revolution due to the transition from bulky devices to miniature, flat and integrated solutions. Integrated flat-optics devices are a new class of optical systems that perform the functions of lenses, diffraction gratings, polarizers, and other elements, but in an ultrathin form factor compatible with microelectronics and photonic chips. Their key feature is the ability to dynamically control optical functions (focusing, beam direction, polarization) in response to external stimuli, including electric field, temperature, light, and mechanical deformations [1]. Integrated flat optics with controlled functions is promising not only for photonics, but also for related fields, from robotics to biosensors, making optical systems more accessible, universal and intelligent by simplifying optical circuits, reducing the size, weight and cost of systems.

Among electro–optical functional materials promising for the creation of flat-optics devices, liquid crystals (LCs) occupy a special place. The unique physical characteristics and the possibility of their control using external electric fields have predetermined the widespread practical use of liquid crystal

media in modern photonics applications. The uniqueness of the LC properties is determined primarily by the relatively high birefringence compared to other electro–optical materials. The high optical anisotropy has also defined the exceptional design parameters of LC devices, whose production relies on thin-film technologies (< 10 μm), which in turn has made these media the most promising electro–optical materials in terms of low energy consumption. Low voltages (units of volts) are required to LC-based control the characteristics of light beams. The tremendous progress in LC display technology has enabled the development of numerous new optical devices for various photonic applications. The development of modern technologies for establishing the initial microstructured orientation of the LC director, based on the photoorientation of polymer materials and azo dyes [2, 3], has enabled the fabrication of a range of photonic LC devices with complex topologies of optical anisotropy. Spatially structured LC components, such as coaxial optical attenuators, polarization controllers, and phase plates, are already available on the market [4, 5]. Liquid crystal devices with a thickness of several microns can be integrated into compact systems such as smartphone cameras, quantum computing chips, etc [6–11].

Currently, special attention is being paid to the development of active diffraction optical elements based on liquid crystals that implement spatial control, multiplexing, polarization and phase transformation of light fields [12–22], which makes them promising functional photonic elements that meet the key requirements of modern laser technologies (telecommunications, medicine, quantum computing, defense systems, etc.). A key requirement in these areas is the precise control of laser radiation parameters: intensity, phase, polarization, and spatial distribution. Traditional optical elements (e.g., static phase plates or diffraction gratings) have fixed characteristics that limit their flexibility. Controlled liquid crystal elements with dynamically adjustable parameters eliminate this limitation, enabling real-time adaptation of the system's optical properties without mechanical motion.

To date, various types of electrically controlled diffraction liquid crystal elements have been developed that operate on a periodically modulated phase of a light wave determined by the topology of a two-domain microperiodic LC director distribution [12–15, 17, 23–28]. Such elements are thin phase gratings (Raman–Nath mode), which limit the diffraction efficiency (40%). Unlike phase diffraction LC gratings, which periodically change the dynamic phase of light, polarization LC gratings periodically modulate the geometric phase, or Pancharatnam–Berry phase, by periodically spatially changing the anisotropy parameters in the plane of the diffraction elements [29, 30]. Such gratings can dynamically adjust the diffraction efficiency under the influence of voltage, reaching a maximum diffraction efficiency of 100% for circularly polarized light [31–38]. Such elements have excellent prospects for application in laser systems, adaptive optics, AR/VR and telecommunications, etc. [34–37]. Moreover, LC elements have several advantages over metasurfaces [39], including a low control voltage below 5 V and low fabrication cost. The LC technology does not require complex and expensive subwavelength patterning [40] that is typical for metasurfaces, simplifying its array scaling and integration into low-voltage dynamic control systems.

In the work, an experimental and theoretical diffraction properties analysis of the electrically controlled polarization liquid crystal twist grating is proposed. Such an LC element is a flat, thin-film, functionally electrically controlled system integrated into a single liquid crystal cell, replacing several static devices in its functionality: a polarizer, a phase plate, and a diffraction grating, with electrically tunable optical characteristics and the ability to switch the spatial frequency of the diffraction structure. The boundary conditions (first proposed in [38]) for the orientation of the LC director in the element permit the formation of a twist structure in the liquid crystal volume, periodic in the angle of rotation. The results provide a comprehensive analytical description of the element's operation under electrical control, as evidenced by the distribution of light intensity across diffraction orders.

The effect of the control voltage on such a LC element allows not only to continuously change its optical phase shift, smoothly changing the polar angle of the director, but also to change the distribution of the nematic liquid crystal (NLC) in the volume of the functional layer, which allows to control the value of diffraction efficiency and to switch the period of the diffraction structure.

2 | Results

2.1 | Electro-Optical Properties of the Twist Polarization Grating

An electrically controlled diffraction grating is formed in a layer of nematic liquid crystal in a sandwich-type element (Figure S1) [41]. The thickness of the homogeneous air gap d, which was subsequently filled with NLC in the isotropic phase, was set by spherical spacers with a diameter of 10 μm (Figure 1). During the fabrication of the element, two glass substrates with a uniform transparent conductive coating of indium tin oxide (ITO) were used, on the inner surfaces of which thin (20–30 nm) orienting layers were previously applied to provide the initial orientation of the director of the liquid crystal layer by setting boundary conditions. To achieve a homogeneous planar orientation, a layer of rubbed Nylon-6 polymer was applied to one of the substrates [42]. A layer of a photoorientant based on the azo dye AtA-2 was applied to the second ITO glass substrate. The formation of an azimuthal orienting LC interaction pattern on the surface of AtA-2 thin films was carried out by photoexposing (Figure S2) a glued cell using the polarization-holographic method [38, 43], implemented according to the Leith–Upatnieks scheme [44] with orthogonal circular polarizations in beams ($\lambda =$ 450 nm) (Figure 1a). In this case, initial boundary conditions are formed on the surface of the photoorientant, representing a periodic dependence of the azimuthal orientation angle of the director $\Phi(x)$. Under these cell boundary conditions, a periodic twist structure with an angle of rotation of the twist $\varphi(x)$ is formed in the volume of the LC layer (Figure 1b).

Figure 2 shows the distribution structure of the LC director in the volume of the functional layer of the photonic element. The period of the created twist periodic structure is determined by rotating the azimuthal angle in the volume by the value $\Delta\varphi(x) = 2\pi$ (Figure 2a). Figure 2b presents a polarizing photograph of the

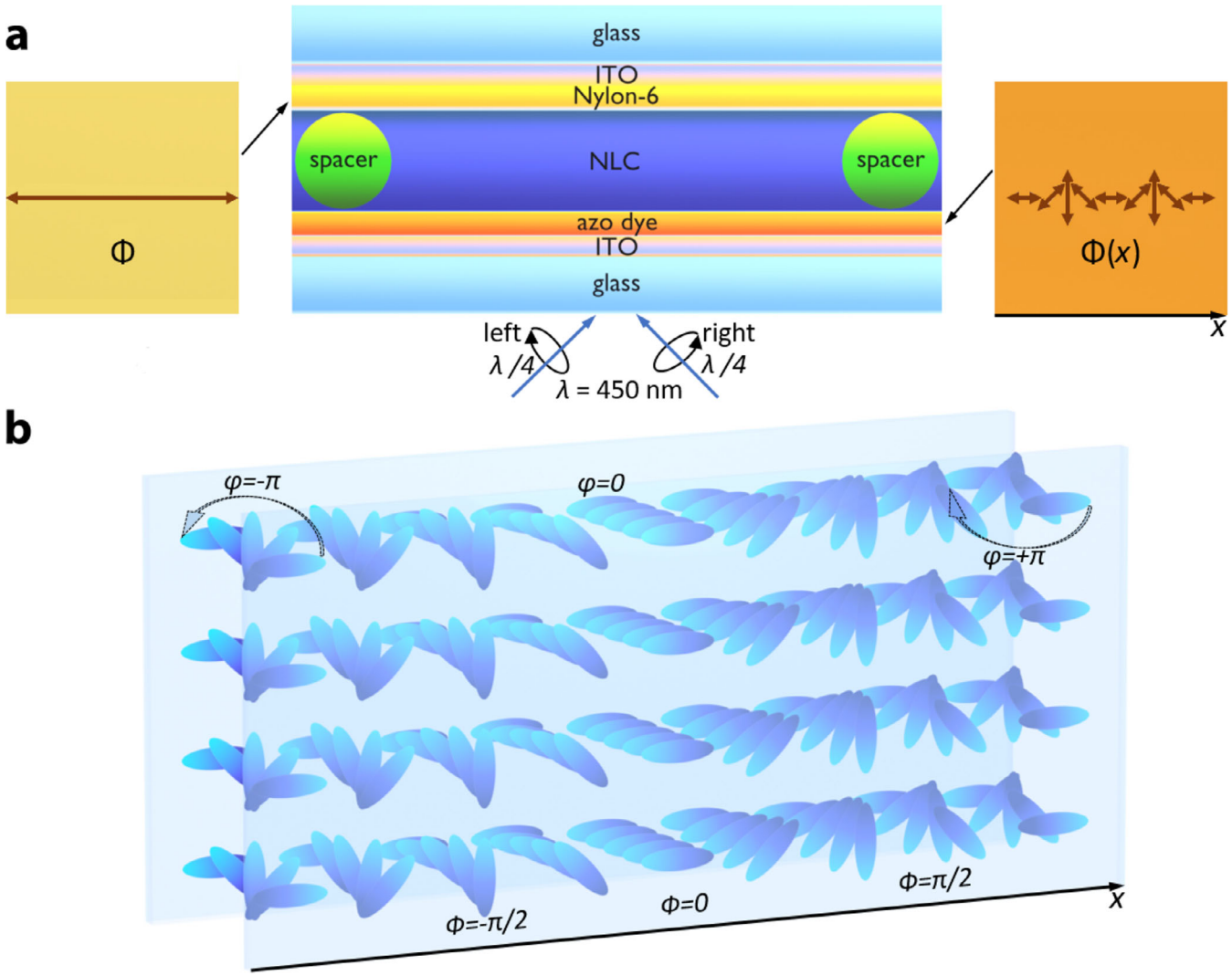

FIGURE 1 | (a) Schematic diagram of the NLC element. The arrows indicate the topology of the boundary conditions for the director of the NLC layer. (b) The orientation distribution of the LC director in the polarizing diffraction structure.

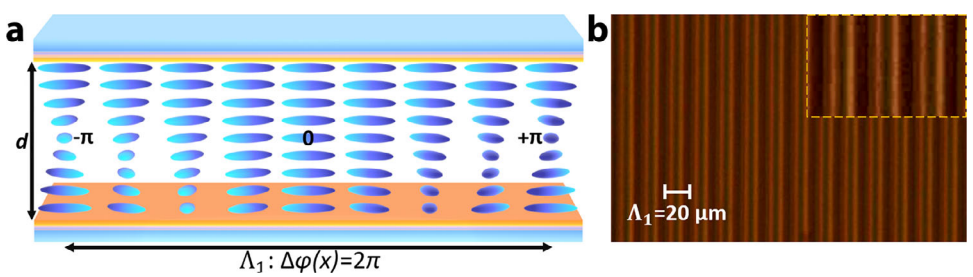

FIGURE 2 | The orientation distribution of the NLC director (a) and micrographs of the polarizing diffraction LC element in crossed polarizers (b) without external control voltage ($U = 0$ V). The inset is showing a zoomed-out pattern of the element.

element in crossed polarizers. When linearly polarized radiation ($\boldsymbol{E} \parallel X$) passes through the twisted regions, the polarization vector of the light rotates after the director, which leads to a rotation of the plane of polarization of the incoming light by an angle φ [41]. For zones with a planar orientation of the NLC director ($\varphi = 0$), the polarization state remains unchanged. Thus, when the polarizer and analyzer are crossed, areas with planar homogeneous ($\varphi = 0$) and twisted by $\varphi = \pm\pi$ director orientations in the NLC layer appear dark in the microscope. The bright areas correspond to twist domains with a director twisting at an angle of $\varphi = \pm\pi/2$.

However, for the twisted structure of the LC, only the volume of the periodic section itself is inseparable, and at each boundary

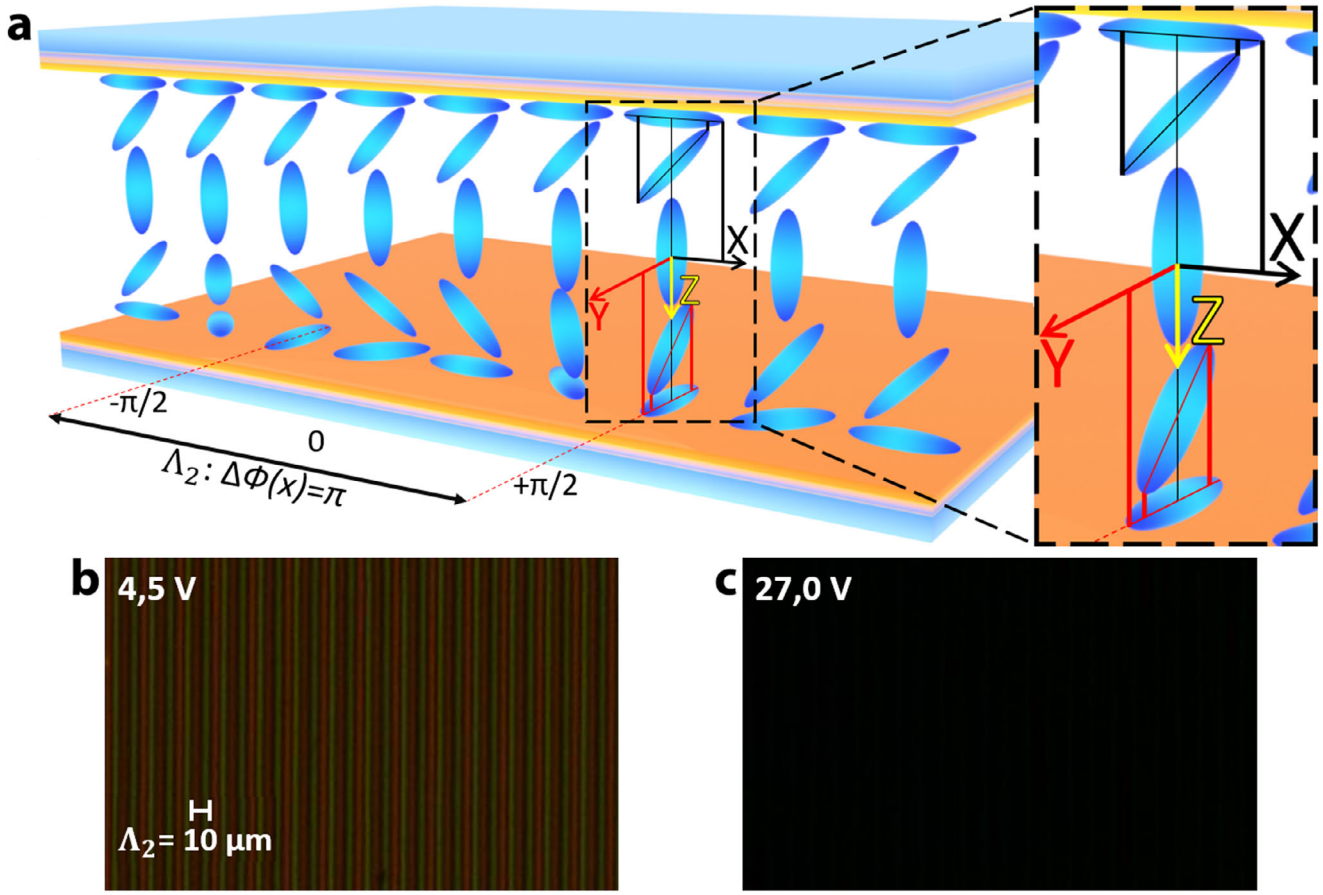

FIGURE 3 | (a) The orientation distribution of the NLC director when the control voltage exceeds the optical threshold value. The inset shows a zoomed-out pattern of the structure. Micrographs of the polarizing diffraction LC element in crossed polarizers under external control voltage $U = 4.5$ V (b), $U = 27.0$ V (c).

between neighboring sections in the volume of the LC there is a topological disclination [45, 46] in the form of a line separating the periods (Figure 2b). This line violates the orientation of the liquid crystal, which separates and stabilizes the boundaries between regions with opposite rotation signs, where the angle of rotation changes abruptly from $-\pi$ to $+\pi$. Therefore, a photonic element with a twisted LC structure has periodic defects, similar to those inherent in Fresnel optics, for example, a Fresnel lens [47].

The transformation of the NLC director orientation topology in the LC layer volume under the action of an electric field leads to the diffraction structure period decrease (Figure 3 and Figure S5). When an external electric voltage is applied, the twist structure of the LC begins to unwind due to the orientation of the NLC molecules' dipole moments along the electric field lines (Fredericks transition [41, 48]). In this case, an LC with a positive anisotropy of dielectric permittivity ($\Delta\epsilon > 0$) is reoriented along the field, which is accompanied by a decrease in the phase shift of the LC layer. When the voltage exceeds the optical threshold value of the twist effect ($U_{th} \approx 2.5$ V), the director in the center of the LC layer rises orthogonally to the substrate (homeotropic orientation), which leads to a complete unwinding of the twist structure and the formation of two independent sublayers in the LC element (Figure 3). The upper liquid crystal sublayer is characterized by the uniformity of the azimuthal orientation angle and the dependence of the polar orientation angle of the director in the plane XZ $\theta(z)$ ($\theta \in [\pi/2, 0]$, hybrid orientation). In the lower NLC sublayer, the director's orientation is a periodic hybrid director's orientation with a varying azimuthal angle $\Phi(x)$ with a period of π (Figure 3a). When linearly polarized radiation ($\boldsymbol{E} \parallel X$) passes through the lower region, birefringence will appear in the domains $\Phi(x) \neq 0$ and $\Phi(x) \neq \pm\pi$, while one polarization mode will propagate in the upper layer.

Figure 3b shows a photograph of the element in crossed polarizers at a voltage value 4.5 V on the cell. For zones with the NLC director initially oriented in the plane, the polarization state remains unchanged. When the polarizer and analyzer are crossed, areas with planar ($\Phi(x) = 0$ and $\Phi(x) = \pm\pi$) director orientations in the NLC layer are visualized in the microscope as dark areas. The colored areas correspond to the orientation of the director $\Phi(x) \neq 0$ and $\Phi(x) \neq \pm\pi$. A further increase in voltage (Figure 3c) leads to a complete reorientation of LC molecules from a planar position (along the surface of the substrates) to a homeotropic position (perpendicular to the surface of the substrates).

2.2 | Description of the Element Operation

In general, the function of any optical system is to affect the transmitting light. If we define the light vector entering the optical system as $\boldsymbol{E}_{input}$, and the light vector exiting the optical system

as $\boldsymbol{E}_{output}$, then we can write the matrix equation:

$$\boldsymbol{E}_{output} = \mathbf{M}_{system}\boldsymbol{E}_{input}, \tag{1}$$

where $\mathbf{M}_{system}$ is the matrix of the optical system operator corresponding to the functional effect of the photonic element on the light vector [49].

To determine the optical function of an electrically controlled photonic element when polarized light propagates through its optical system, we use the formalism of the 2×2 matrix method of Jones matrices [50]. It is convenient to represent the entering circularly polarized light vector in a general way as:

$$\boldsymbol{E}_{input} = \frac{1}{\sqrt{2}}\begin{bmatrix}1\\-i\sigma\end{bmatrix}, \tag{2}$$

where σ takes the values +1 and –1 for the right and left circular polarizations, respectively.

At low voltage levels (U), a twisted nematic LC cell is an equivalent optical circuit of a photonic element, where rubbing on the upper substrate sets the zero azimuthal direction, and the local rotation angle of the LC is determined by the photoorientant as $\varphi(x)$. In the case of a periodically-continuously changing azimuthal direction of photoorientation (obtained by exposing crossed beams of circularly polarized laser radiation), the rotation angle of the LC can take values from –180° to +180°, i.e. $\varphi(x) \in [-\pi, \pi]$, due to minimization of the volumetric energy of LC elastic deformation and anchoring energy on the surface. The optical phase shift of the element $\delta_1(U)$ (Figure S6) depends on the applied voltage.

In this case, the matrix of the operator $\mathbf{M}_{system}$ corresponding to the photonic element can be represented as the Jones matrix of the twist-nematic LC cell [50]:

$$\mathbf{M}_{system}(x,U) = \begin{bmatrix}a(x,U) - ib(x,U) & -c(x,U) - id(x,U)\\ c(x,U) - id(x,U) & a(x,U) + ib(x,U)\end{bmatrix}, \tag{3}$$

where $\chi(x,U) = \sqrt{\varphi(x)^2 + \delta_1(U)^2}$,

$a(x,U) = \cos(\chi(x,U))\cos(\varphi(x)) + \frac{\varphi(x)}{\chi(x,U)}\sin(\chi(x,U))\sin(\varphi(x))$,

$b(x,U) = \frac{\delta_1(U)}{\chi(x,U)}\sin(\chi(x,U))\cos(\varphi(x))$,

$c(x,U) = \cos(\chi(x,U))\sin(\varphi(x)) - \frac{\varphi(x)}{\chi(x,U)}\sin(\chi(x,U))\cos(\varphi(x))$,

$d(x,U) = \frac{\delta_1(U)}{\chi(x,U)}\sin(\chi(x,U))\sin(\varphi(x))$,

$\delta_1(U) = \frac{\pi}{\lambda}\Delta n(U)d$ - optical phase shift of the LC cell,

λ - wavelength,

d - thickness of the NLC cell layer,

$\Delta n(U)$ - anisotropy of the refractive index,

U - the value of the external applied voltage on the element.

Then the output light vector $\boldsymbol{E}_{output}(x,U)$ is a function of the applied voltage U and the spatial coordinate x, and can be found as follows:

$$\begin{aligned}\boldsymbol{E}_{output}(x,U) &= \mathbf{M}_{system}(x,U)\boldsymbol{E}_{input}\\ &= \begin{bmatrix}a(x,U) - ib(x,U) & -c(x,U) - id(x,U)\\ c(x,U) - id(x,U) & a(x,U) + ib(x,U)\end{bmatrix}\frac{1}{\sqrt{2}}\\ &\times\begin{bmatrix}1\\-i\sigma\end{bmatrix} = \frac{1}{\sqrt{2}}\begin{bmatrix}1\\-i\sigma\end{bmatrix}\cos(\delta_1(U))e^{i\sigma\varphi(x)}\\ &+\frac{1}{\sqrt{2}}\begin{bmatrix}1\\i\sigma\end{bmatrix}e^{-i\pi/2}\sin(\delta_1(U))e^{-i\sigma\varphi(x)}.\end{aligned} \tag{4}$$

At the output of a photonic element with a twisted LC structure, there are two vectors with right and left circular polarization – the eigenvectors of the twisted LC structure (Figure 1b). The amplitudes of these output light vectors are determined by the polarization of the input light and the optical phase of the twisted nematic LC layer of the photonic element $\delta_1(U)$, and for each point with the spatial coordinate x, the phase of the vectors is determined by the spatial distribution of the rotation angle of the LC $\varphi(x)$. Moreover, the local rotation angle is determined by the azimuthal photoalignment direction, a geometric factor that sets the multipliers of the geometric phase $e^{i\varphi(x)}$ and $e^{-i\varphi(x)}$ for the right and left circular polarization of the light vectors at the output of the photonic element, respectively.

It is important to note that it is the pattern of the azimuthal photoalignment directions $\Phi(x)$ that determines the propagation directions of the output vectors. Thus, with a linear dependence of $\Phi(x)$, the LC structure forms periodic sections with a period of Λ_1, where the azimuthal angle of photoorientation experiences a 360° rotation. Such spatially periodic regions are distinguishable when observing the element in a polarizing microscope with crossed polarizers (Figure 2b). At each periodic segment, the rotation angle of the LC increases linearly from $-\pi$ to $+\pi$, which corresponds to a linear increase in the geometric phase by 2π. Such a linear distribution of the geometric phase corresponds to two phase profiles of two inclined planes type [29], where the angle of plane inclination depends on the σ-polarization of the incident light, the wavelength of the light λ and the period of the twisted LC structure Λ_1, and the sign "+" or "–" of the angle of plane inclination depends on the phase multiplier $e^{i\varphi(x)}$ or $e^{-i\varphi(x)}$, respectively. The light diffraction on such a periodic twisted LC structure of a photonic element is equivalent to the refraction of light on an inclined flat interface; therefore, the outgoing light vectors with right and left circular polarization propagate, respectively, in ±1 diffraction orders.

It is possible to adjust the optical phase $\delta_1(U)$ when controlling the applied voltage level, and therefore controlling the intensity ratio of the output vectors diffracting in the +1 and –1 orders (Table S1).

An increase in the voltage at the cell electrodes, typically more than > 2.5 V, leads to an excess of the polar angle of inclination of the director in the cell center to a critical value (vertical

orientation), at which the homogeneity of the twist of the LC structure is disrupted (Figure 3a). This is accompanied by the unwinding of the liquid crystal due to the loss of coupling between the upper and lower cell substrates [51] through elastic twist deformation of the LC material. The optical scheme of such an LC cell is a system of two independent phase retarders [52], the axes azimuthal directions of which are set by an orientant (Nylon-6) and a photoorientant (AtA-2) on the upper and lower substrates of the cell, respectively. At the same time, both system retarders have the same optical phase value $\delta(U)$ (Figure S7), determined by the residual birefringence of the liquid crystal surface sublayer, which depends on the liquid crystal parameters, the LC cell gap and the applied voltage.

In the Jones matrix formalism, the general view of the $\mathbf{M}_{system}$ matrix of a system with an untwisted LC structure (at voltage above > 2.5 V) is two identical phase retarders rotated at each point x at angles $\alpha_1(x)$ and $\alpha_2(x)$, respectively, and has the following form:

$$\mathbf{M}_{system}(x,U) = \mathbf{R}(-\alpha_2(x))\mathbf{M}_{\delta(U)}\mathbf{R}(\alpha_2(x))\mathbf{R}(-\alpha_1(x))\mathbf{M}_{\delta(U)}\mathbf{R}(\alpha_1(x)), \quad (5)$$

where $\mathbf{M}_{\delta(U)} = \begin{bmatrix} e^{-i\delta(U)} & 0 \\ 0 & e^{i\delta(U)} \end{bmatrix}$ is matrix of a phase retarder with a $\delta(U)$ phase shift,

$\mathbf{R}(\alpha) = \begin{bmatrix} cos(\alpha) & sin(\alpha) \\ -sin(\alpha) & cos(\alpha) \end{bmatrix}$ is the rotation matrix.

The diffraction-order distribution of the output light intensity depends on the side of the element through which the input enters (from the Nylon-6 or AtA-2 side) and on the optical phase, set by the applied voltage. When σ-circularly polarized light enters the system from the side of the substrate with the orientant Nylon-6, its orientation is selected for the zero direction, and the azimuthal angle of photoorientation can take values in the range from –90° to +90°, i.e. $\Phi(x) \in [-\pi/2, \pi/2]$, its direction sign corresponds to the rotation angle $\varphi(x)$. Therefore, when determining the matrix of the system (Equation (5)), choose $\alpha_1(x) = 0$ and $\alpha_2(x) = \Phi(x)$. The light vector $\boldsymbol{E}_{output}(x,U)$ behind the element will have the form:

$$\begin{aligned}\boldsymbol{E}_{output}(x,U) &= \mathbf{M}_{system}(x,U)\boldsymbol{E}_{input} \\ &= \begin{bmatrix} cos(\Phi(x)) & -sin(\Phi(x)) \\ sin(\Phi(x)) & cos(\Phi(x)) \end{bmatrix} \begin{bmatrix} e^{-i\delta(U)} & 0 \\ 0 & e^{i\delta(U)} \end{bmatrix} \\ &\times \begin{bmatrix} cos(\Phi(x)) & sin(\Phi(x)) \\ -sin(\Phi(x)) & cos(\Phi(x)) \end{bmatrix} \begin{bmatrix} e^{-i\delta(U)} & 0 \\ 0 & e^{i\delta(U)} \end{bmatrix} \\ &\times \frac{1}{\sqrt{2}} \begin{bmatrix} 1 \\ -i\sigma \end{bmatrix} = \frac{1}{\sqrt{2}} \begin{bmatrix} e^{-i\delta(U)} \\ -i\sigma e^{i\delta(U)} \end{bmatrix} \cos(\delta(U)) \\ &+ \frac{1}{\sqrt{2}} \begin{bmatrix} 1 \\ -i\sigma \end{bmatrix} sin^2(\delta(U)) e^{\pm i\pi} e^{2i\sigma\Phi(x)} \\ &+ \frac{1}{2\sqrt{2}} \begin{bmatrix} 1 \\ i\sigma \end{bmatrix} sin(2\delta(U)) e^{-i\pi/2} e^{-2i\sigma\Phi(x)}. \end{aligned} \quad (6)$$

The outgoing light is distributed between three vectors with geometric phase multipliers $1 \equiv e^{0i}$, $e^{2i\Phi(x)}$ and $e^{-2i\Phi(x)}$, which corresponds to diffraction of light in the 0 and $\pm 1'$ orders (Table S2).

To study the diffraction properties of the fabricated LC cell, experimental setups were used (Figure 4), including a He-Ne laser generating a narrow beam of light with a wavelength of 632.8 nm, a collimating system consisting of a 20X objective and a lens (f = 20 cm), a Wire Grid polarizer, a quarter-wave phase plate $\lambda/4$, and a generator of variable rectangular-shaped signals (with a frequency of 1 kHz), a complementary metal-oxide-semiconductor (CMOS) camera and a power meter that records the intensity of radiation diffracted into the m diffraction order. The values of the diffraction efficiency η_m (in %), characterizing the energy distribution of transmitted light in diffraction orders m, were calculated using the formula $\eta_m = \frac{I_m}{I_0} \cdot 100\%$, where I_m is the intensity of the light beam in the m diffraction order; I_0 is the total intensity of light leaving the element.

Figure 5 presents the experimental and theoretical results of a study of the diffraction efficiencies (η_m) dependence on the external control voltage U when light enters the system from the Nylon-6 side (λ = 632.8 nm).

When σ-circularly polarized light enters the system from the side of the photoorientant AtA-2 substrate, the azimuthal photoorientation angle can take values in the range from –90° to +90°, i.e. $\Phi(x) \in [-\pi/2, \pi/2]$, therefore, when determining the matrix of the system (Equation (5)) choose $\alpha_1(x) = \Phi(x)$, and $\alpha_2(x) = 0$. The light vector $\boldsymbol{E}_{output}(x,U)$ behind the element is written as:

$$\begin{aligned}\boldsymbol{E}_{output}(x,U) &= \mathbf{M}_{system}(x,U)\boldsymbol{E}_{input} \\ &= \begin{bmatrix} e^{-i\delta(U)} & 0 \\ 0 & e^{i\delta(U)} \end{bmatrix} \begin{bmatrix} cos(\Phi(x)) & -sin(\Phi(x)) \\ sin(\Phi(x)) & cos(\Phi(x)) \end{bmatrix} \\ &\times \begin{bmatrix} e^{-i\delta(U)} & 0 \\ 0 & e^{i\delta(U)} \end{bmatrix} \begin{bmatrix} cos(\Phi(x)) & sin(\Phi(x)) \\ -sin(\Phi(x)) & cos(\Phi(x)) \end{bmatrix} \\ &\times \frac{1}{\sqrt{2}} \begin{bmatrix} 1 \\ -i\sigma \end{bmatrix} = \frac{1}{\sqrt{2}} \begin{bmatrix} e^{-i\delta(U)} \\ -i\sigma e^{i\delta(U)} \end{bmatrix} \cos(\delta(U)) \\ &+ \frac{1}{\sqrt{2}} \begin{bmatrix} -ie^{-i\delta(U)} \\ \sigma e^{i\delta(U)} \end{bmatrix} sin(\delta(U)) e^{-2i\sigma\Phi(x)}. \end{aligned} \quad (7)$$

The outgoing light is distributed between two vectors with geometric phase multipliers $1 \equiv e^{0i}$ and $e^{2i\sigma\varphi(x)}$, which corresponds to diffraction of light in the 0 and $1'\sigma$ orders (Table S2).

The dependences of diffraction efficiencies in the 0 and $1'\sigma$ diffraction orders on the control voltage U on the element when diffraction of a circularly polarized wave for this case (entrance from AtA-2) are shown in Figure 6.

Effective electrical control of the director orientation topology within the NLC volume enables a controlled change in the diffraction properties of the twist-planarly oriented polarization grating. Figure 7 presents photographs of diffraction patterns of circularly polarized He-Ne laser radiation at different control voltage amplitude levels. Circularly polarized radiation diffracts

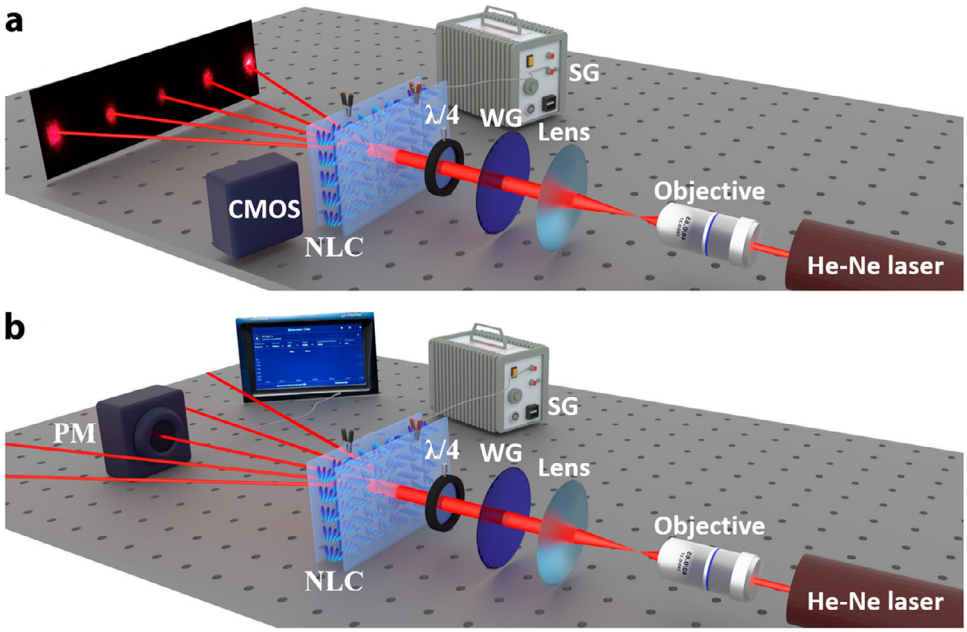

FIGURE 4 | Schemes of experimental setups for recording diffraction patterns (a) and measuring the intensity (b) of a diffracted circularly polarized light field on the NLC element with a He-Ne laser $\lambda = 632.8$ nm, a 20X objective, a spherical lens, a Wire Grid polarizer (WG), a quarter-wave phase plate ($\lambda/4$), a nematic liquid crystal cell (NLC), CMOS camera, power meter (PM) and a generator of variable signals (SG).

asymmetrically from the element in opposite directions of polarization rotation (left and right). In the absence of voltage ($U = 0$ V), the NLC structure operates in the twist mode of the diffraction grating with a period of $\Lambda_1 = 20\,\mu$m. An increase in the control voltage on the element ($U > 2.5$ V) leads to a switching of the period of the diffraction structure $\Lambda_2 = 10\,\mu$m (Figure 3). Another feature of the proposed polarizing photonic device is the ambiguity in the diffraction efficiency relative to the input radiation, whether from the Nylon-6 or AtA-2 side. Experimental diffraction patterns emphasize the high efficiency of the element, its sensitivity to the direction of rotation of circularly polarized light and to the side of the radiation entrance into the element.

3 | Conclusion

The article presents a deep understanding of the structure functioning under applied voltage for an electrically controlled diffraction NLC twist element based on the geometric Pancharatnam–Berry phase.

An electrically induced switch in the diffraction grating period has been demonstrated experimentally and theoretically. The polarizing photonic element, created with an initially twisted structure, enables electrical control of the diffraction efficiency (an experimental value of 91% has been achieved) and of the LC structure's period, which determines the diffraction direction. Switching between diffraction orders is demonstrated when the polarization of the beam incident on the NLC cell changes from left-circular to right-circular and when the radiation passage sequence of the NLC orienting layers (AtA-2 and Nylon-6) changes.

The results obtained open up new possibilities for the design and application of complex planar electrically controlled diffraction NLC elements based on the geometric Pancharatnam–Berry phase in multifunctional flat optical devices and systems.

4 | Experimental Section

The proposed electrically switchable photonic device is a layer of NLC 1282 (NIOPIK, Russia) with a thickness of $d = 10\,\mu$m, placed between a lower substrate with an azimuthal angle of the planar orientation of the NLC director periodically varying from $-\pi/2$ to $+\pi/2$ and an upper substrate with a uniform planar alignment of molecules. Under the influence of hybrid director alignment, NLC molecules form a reconfigurable topological optical phase-diffraction structure with a controllable period.

The corpus of the sandwich-type [41] element was made using two 1.1 mm thick glass substrates with transparent solid ITO electrodes with a resistance of 100 ohm sq^{-1} (Integral OJSC, Minsk, Belarus) to electrically change the distribution structure of the mesogenic layer and, accordingly, the optical phase of the structure. The preliminary cleaning of the inner substrate surfaces took place in several successive stages: ultrasonic cleaning in an aqueous solution of a surfactant in distilled water; UV cleaning of organic pollutants (Photo Surface Processor PL16-110D, SEN LIGHTS Corp., JP); removal of organic pollution traces and dust particles with compressed air (compressor Remeza CJSC, Minsk, Belarus). Liquid deposition of ultrathin orienting films with a thickness of about 20–30 nm on the surface of thoroughly cleaned glass substrates was carried out using the Mayer–Rod Coating method.

Nylon-6 [53] was chosen as the orienting material for setting the homogeneous planar orientation of the NLC director, the film of which was rubbed after coating on the substrate. A film of photosensitive azo dye AtA-2 (MTLCD lab) was applied to the

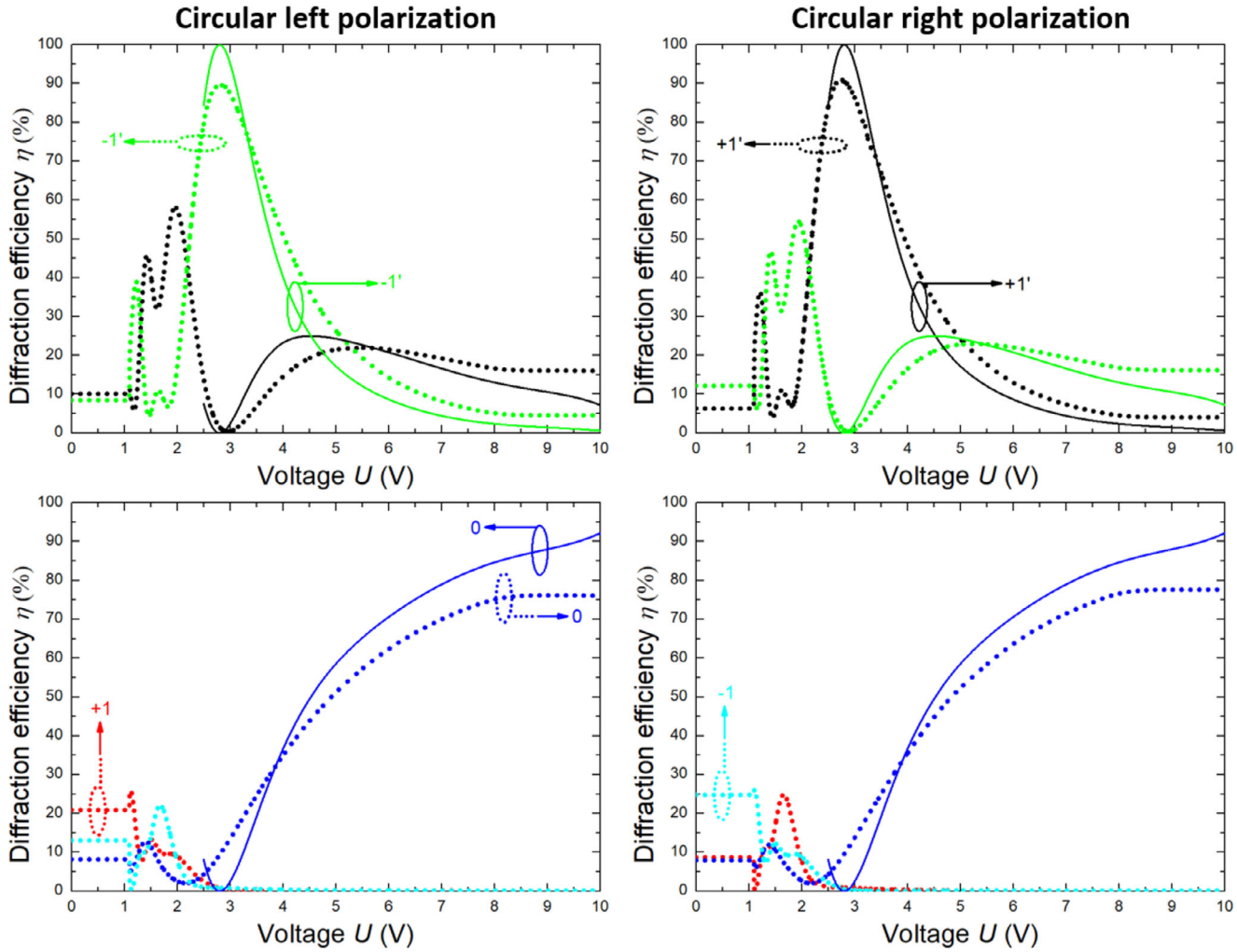

FIGURE 5 | Experimental (dotted lines) and theoretical (straight lines) dependences of the diffraction efficiency of the LC element on the voltage for circular (left and right) polarization when light enters the system from the Nylon-6 side ($\lambda = 632.8$ nm). Note: The lines representing the results corresponding to different diffraction orders are indicated in different colors: $+1'$ diffraction order is black, +1 is red, 0 is blue, –1 is light blue, $-1'$ is green.

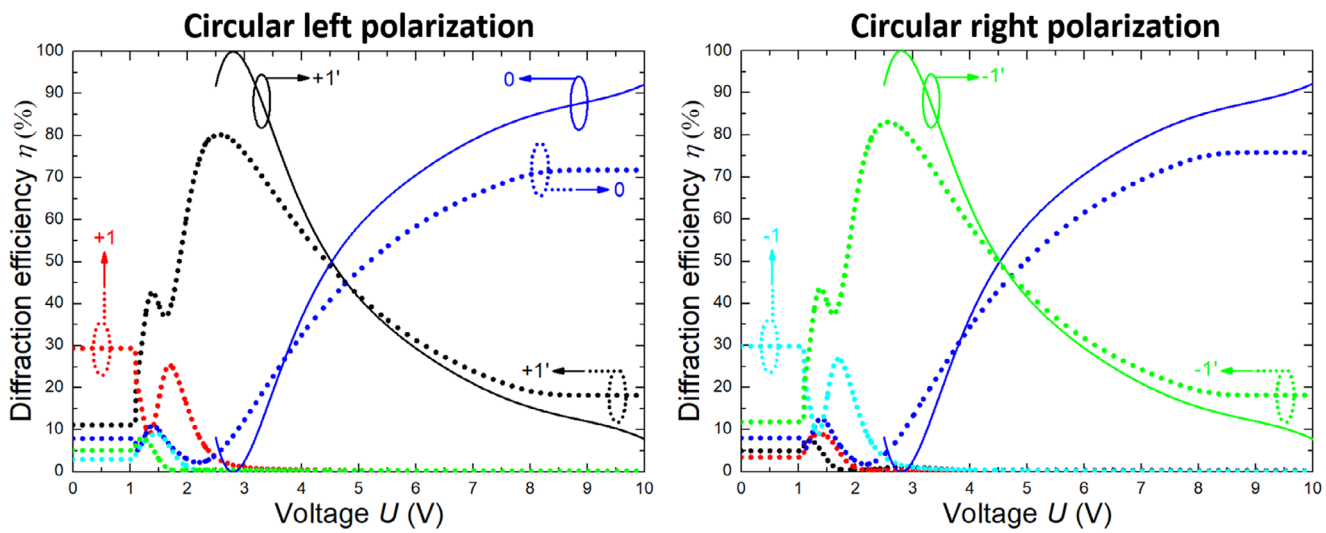

FIGURE 6 | Experimental (dotted lines) and theoretical (straight lines) dependences of the diffraction efficiency of the LC element on the voltage for circular (left and right) polarization when light enters the system from AtA-2 ($\lambda = 632.8$ nm). Note: The lines representing the results corresponding to different diffraction orders are indicated in different colors: $+1'$ diffraction order is black, +1 is red, 0 is blue, –1 is light blue, $-1'$ is green.

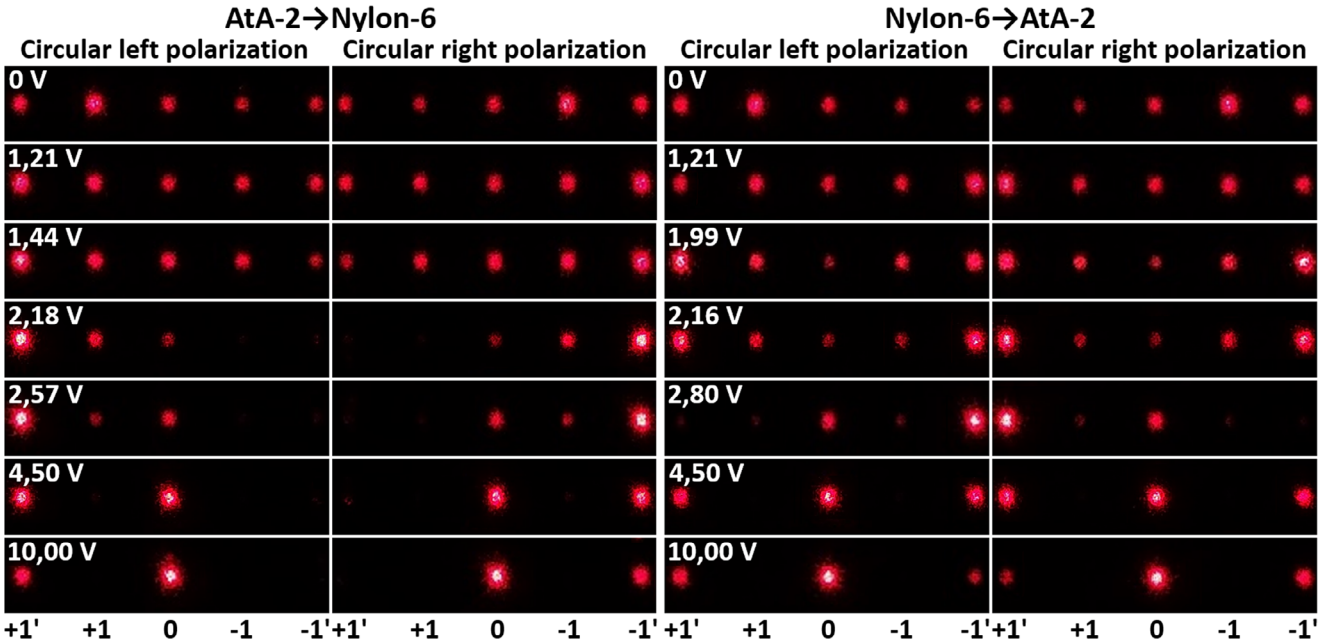

FIGURE 7 | Photographs of diffraction patterns of circularly (left and right) polarized radiation on the NLC element when the external control voltage on the LC cell changes and when the orientation layers are sequentially transmitted by the radiation: AtA-2 → Nylon-6 or Nylon-6 → AtA-2.

second substrate, which provides a strong azimuthal anchoring energy (values of the azimuthal anchoring energy constant $\sim 2.4 \cdot 10^{-4}$ J m^{-2} [54]). The ability of photoorientation by the mechanism of photoinduced hole dipoles without birefringence induction in a thin film of AtA-2 azo dye when exposed to radiation with a wavelength of 450 nm makes it possible to obtain optically correct NLC phase distributions [55, 56], which makes the applied photoalignment material suitable for the creation of photonic devices based on geometric phase (Pancharatnam-Berry phase). The orienting properties of AtA-2 film are formed after its exposure to linear polarization radiation. The photoexposure of the azo dye was carried out after the assembly of the NLC cell of the photonic device by radiation resulting from the coherent addition of two circularly orthogonally polarized beams with a wavelength of $\lambda = 450$ nm (Figure S2). The power density was $I = 15$ mW cm^{-2}. After exposure, the capillary gap with a thickness of $d = 10$ μm was filled with nematic LC 1282 in the isotropic phase in a vacuum drying cabinet (Memmert VOcool 400).

The LC Structure program [57] was used for a model approximation of the dependence of optical phases on voltage $\delta(U)$, $\delta_1(U)$ (Figures S6 and S7). For this purpose, the characteristic voltage transmission curves $T(U)$ (Figures S3 and S4), were calculated for antiparallel and twist (with 90° twist) cells with a thickness of $d = 10.6$ μm filled with liquid crystal LC 1282, NIOPIC ($K_{11} = 10.4$ pN, $K_{22} = 4.2$ pN, $K_{33} = 11.5$ pN, $\Delta\epsilon = 11.0$, $\epsilon_{\parallel} = 5.6$, $\Delta n = 0.17$ for a wavelength of 632 nm at room temperature +20 °C). The orientation direction axes of the antiparallel LC cell and the orientation direction on one of the twist cell substrates were 45° to the input polarizer crossed to the output analyzer. We considered the normal incidence of light. In such a geometry, the required optical phase $\delta(U)$ at a voltage > 2.5 V is equivalent to half the phase shift of the antiparallel LC cell, and can be estimated as: $\delta(U) = \frac{1}{2}\arcsin\sqrt{T(U)}$. While $\delta_1(U)$ at a voltage of < 2.5 V is equivalent to the phase shift of a twist cell: $\delta_1(U) = \sqrt{\arcsin^2\sqrt{T(U)} - \Phi^2}$ at the angle of rotation of the LC $\Phi = \pi/2$.

Acknowledgements

The research was supported by the Israel Science Foundation ISF no. 1023/24 and the State program of scientific research "Photonics and Electronics for Innovation".

Conflicts of Interest

The authors declare no conflicts of interest.

Data Availability Statement

The data that support the findings of this study are available from the corresponding author upon reasonable request.

Conflicts of Interest

The authors declare no conflict of interest.

References

1. Q. Wang, E. T. Rogers, B. Gholipour, et al., "Optically Reconfigurable Metasurfaces and Photonic Devices Based on Phase Change Materials," *Nature Photonics* 10, no. 1 (2016): 60–65.

2. V. G. Chigrinov, V. M. Kozenkov, and H.-S. Kwok, *Photoalignment of Liquid Crystalline Materials: Physics and Applications* (John Wiley & Sons, 2008).

3. S. Slussarenko, A. Murauski, T. Du, V. Chigrinov, L. Marrucci, and E. Santamato, "Tunable Liquid Crystal Q-Plates with Arbitrary Topological Charge," *Optics Express* 19, no. 5 (2011): 4085–4090.

4. V. G. Chigrinov, "Liquid Crystal Photonics," in *Liquid Crystal Photonics* (2014), 1–204.

5. D.-K. Yang and S.-T. Wu, *Fundamentals of Liquid Crystal Devices* (John Wiley & Sons, 2014).

6. Z. He, F. Gou, R. Chen, K. Yin, T. Zhan, and S.-T. Wu, "Liquid Crystal Beam Steering Devices: Principles, Recent Advances, and Future Developments," *Crystals* 9, no. 6 (2019): 292.

7. Y. Zhou, Y. Yin, Y. Yuan, et al., "Liquid Crystal Pancharatnam-Berry Phase Lens with Spatially Separated Focuses," *Liquid Crystals* 46, no. 7 (2019): 995–1000.

8. J. Zhou, H. Qian, C.-F. Chen, et al., "Optical Edge Detection Based on High-Efficiency Dielectric Metasurface," *Proceedings of the National Academy of Sciences of the United States of America* 116, no. 23 (2019): 11137–11140.

9. T. Lin, T. Zhan, J. Zou, F. Fan, and S.-T. Wu, "Maxwellian Near-Eye Display with an Expanded Eyebox," *Optics Express* 28, no. 26 (2020): 38616–38625.

10. T. Zhan, Y.-H. Lee, G. Tan, et al., "Pancharatnam–Berry Optical Elements for Head-Up and Near-Eye Displays," *Journal of the Optical Society of America B* 36, no. 5 (2019): D52–D65.

11. C. Packham, M. Escuti, J. Ginn, C. Oh, I. Quijano, and G. Boreman, "Polarization Gratings: A Novel Polarimetric Component for Astronomical Instruments," *Publications of the Astronomical Society of the Pacific* 122, no. 898 (2010): 1471.

12. H. Sarkissian, S. V. Serak, N. V. Tabiryan, L. B. Glebov, V. Rotar, and B. Y. Zeldovich, "Polarization-Controlled Switching Between Diffraction Orders in Transverse-Periodically Aligned Nematic Liquid Crystals," *Optics Letters* 31, no. 15 (2006): 2248–2250.

13. M. Bouvier and T. Scharf, "Analysis of Nematic-Liquid-Crystal Binary Gratings with High Spatial Frequency," *Optical Engineering* 39 (2000): 2129–2137.

14. M. Honma and T. Nose, "Temperature-Independent Achromatic Liquid-Crystal Grating with Spatially Distributed Twisted-Nematic Orientation," *Applied Physics Express* 5, no. 6 (2012): 062501.

15. S. Valyukh, V. Chigrinov, H. S. Kwok, and H. Arwin, "On Liquid Crystal Diffractive Optical Elements Utilizing Inhomogeneous Alignment," *Optics Express* 20, no. 14 (2012): 15209–15221.

16. K. Rutkowska, M. Chychłowski, M. Kwa'sny, I. Ostromecka, J. Piłka, and U. Laudyn, "Light Propagation in Periodic Photonic Structures Formed by Photo-Orientation and Photo-Polymerization of Nematic Liquid Crystals," *Opto-Electronics Review* 25, no. 2 (2017): 118–126.

17. M. Nieborek, K. Rutkowska, T. R. Woli'nski, et al., "Tunable Polarization Gratings Based on Nematic Liquid Crystal Mixtures Photoaligned with Azo Polymer-Coated Substrates," *Crystals* 10, no. 9 (2020): 768.

18. E. A. Melnikova, "Electrically Controlled Microstructured Liquid-Crystal Twist Elements for Phase Conversion of Light Fields," *Journal of Optical Technology* 89, no. 3 (2022): 169–175.

19. E. Melnikova, Y. Pantsialeyeva, D. Gorbach, A. Tolstik, and A. Karabchevsky, "Tunable Liquid Crystal Twisted-Planar Fresnel Lens for Vortex Topology Determination," *Laser & Photonics Reviews* 19, no. 4 (2025): 2401006.

20. E. Melnikova, K. Pantsialeyeva, D. Gorbach, A. Tolstik, S. Slussarenko Jr, and A. Karabchevsky, "Phase Topology Stability of an Optical Vortex via an Electrically Controlled Twist-Planar Oriented Liquid Crystal Fresnel Lens," *arXiv Preprint arXiv:2506.02632* (2025).

21. I. Nys, B. Berteloot, and K. Neyts, "Photoaligned Liquid Crystal Devices with Switchable Hexagonal Diffraction Patterns," *Materials* 15, no. 7 (2022): 2453.

22. C. Provenzano, P. Pagliusi, and G. Cipparrone, "Electrically Tunable Two-Dimensional Liquid Crystals Gratings Induced by Polarization Holography," *Optics Express* 15, no. 9 (2007): 5872–5878.

23. S.-Y. Huang, S.-T. Wu, and A. Y.-G. Fuh, "Optically Switchable Twist Nematic Grating Based on a Dye-Doped Liquid Crystal Film," *Applied Physics Letters* 88, no. 4 (2006): 041104.

24. V. Kapoustine, A. Kazakevitch, V. So, and R. Tam, "Simple Method of Formation of Switchable Liquid Crystal Gratings by Introducing Periodic Photoalignment Pattern into Liquid Crystal Cell," *Optics Communications* 266, no. 1 (2006): 1–5.

25. W.-Y. Wu and A. Y.-G. Fuh, "Rewritable Liquid Crystal Gratings Fabricated Using Photoalignment Effect in Dye-Doped Poly (Vinyl Alcohol) Film," *Japanese Journal of Applied Physics* 46, no. 10R (2007): 6761.

26. W. Hu, A. Srivastava, F. Xu et al., "Liquid Crystal Gratings Based on Alternate TN and PA Photoalignment," *Optics Express* 20, no. 5 (2012): 5384–5391.

27. R. Węgłowski, A. Kozanecka-Szmigiel, W. Piecek, J. Konieczkowska, and E. Schab-Balcerzak, "Electro-Optically Tunable Diffraction Grating with Photoaligned Liquid Crystals," *Optics Communications* 400 (2017): 144–149.

28. E. Melnikova, I. Stashkevich, I. Rushnova, A. Tolstik, and S. Timofeev, "Polarization Properties of the Electrically Controlled Twist-Planar Liquid Crystal Diffraction Structure," *Nonlinear Phenomena in Complex Systems* 25, no. 3 (2022): 229–244.

29. V. Y. Stanevich and A. Muravsky, "Liquid Crystal's Photoalignment for Formation of Phase Profiles via Geometric Phase Distribution," *Journal of the Belarusian State University Physics* 3 (2022): 10–25.

30. R. Barboza, U. Bortolozzo, M. G. Clerc, and S. Residori, "Berry Phase of Light under Bragg Reflection by Chiral Liquid-Crystal Media," *Physical Review Letters* 117, no. 5 (2016): 053903.

31. M. J. Escuti and W. M. Jones, "39.4: Polarization-Independent Switching with High Contrast from a Liquid Crystal Polarization Grating," in *SID Symposium Digest of Technical Papers*, vol. 37, no. 1 (Wiley Online Library, 2006), 1443–1446.

32. C. Provenzano, P. Pagliusi, and G. Cipparrone, "Highly Efficient Liquid Crystal Based Diffraction Grating Induced by Polarization Holograms at the Aligning Surfaces," *Applied Physics Letters* 89, no. 12 (2006): 121105.

33. M. Sakamoto, S. Ohara, Y. Mitsuboshi, et al., "Design and Fabrication of a Liquid Crystal Polarization Grating for Mid- and Far-Infrared Wavelengths," *Applied Optics* 63, no. 8 (2024): 2095–2100.

34. D. Xu, Q. Guo, T. Liu, H. Zhao, V. G. Chigrinov, and H. S. Kwok, "P-3.5: An Exposure Method of Liquid Crystal Polarization Grating for VR/AR Optical Systems," in *SID Symposium Digest of Technical Papers*, vol. 52 (Wiley Online Library, 2021), 728–731.

35. G. Zhang, A. Schreier, C. He, et al., "Optical Beam-Steering and Polarization Property of a Liquid Crystal Laser," in *Liquid Crystals XXVII* (SPIE, 2023), PC1265805.

36. E. Nicolescu and M. J. Escuti, "Polarization-Independent Tunable Optical Filters Using Bilayer Polarization Gratings," *Applied Optics* 49, no. 20 (2010): 3900–3904.

37. M. W. Kudenov, M. J. Escuti, E. L. Dereniak, and K. Oka, "White-Light Channeled Imaging Polarimeter Using Broadband Polarization Gratings," *Applied Optics* 50, no. 15 (2011): 2283–2293.

38. G. P. Crawford, J. N. Eakin, M. D. Radcliffe, A. Callan-Jones, and R. A. Pelcovits, "Liquid-Crystal Diffraction Gratings Using Polarization Holography Alignment Techniques," *Journal of Applied Physics* 98, no. 12 (2005): 123102.

39. S. B. Glybovski, S. A. Tretyakov, P. A. Belov, Y. S. Kivshar, and C. R. Simovski, "Metasurfaces: From Microwaves to Visible," *Physics Reports* 634 (2016): 1–72.

40. A. I. Kuznetsov, A. E. Miroshnichenko, M. L. Brongersma, Y. S. Kivshar, and B. Luk'yanchuk, "Optically Resonant Dielectric Nanostructures," *Science* 354, no. 6314 (2016): aag2472.

41. L. Blinov and V. Chigrinov, *Elektro-i Magnitooptika Zhidkikh Kristallov* (Springer New York, 1993).

42. J.-J. Wook and J.-H. Kim, "Imprinting of Liquid Crystal Alignment on Polymer Layers," (2003): 611–614.

43. T. Lin, J. Xie, Y. Zhou, et al., "Recent Advances in Photoalignment Liquid Crystal Polarization Gratings and Their Applications," *Crystals* 11, no. 8 (2021): 900.

44. R. Collier, C. B. Burckhardt, and L. H. Lin, *Optical Holography* (Academic Press, 1971).

45. D. Kasyanyuk, P. Pagliusi, A. Mazzulla, et al., "Manipulation of Colloids by Optical and Electrical Control of Disclination Lines in Liquid Crystals," *Optofluidics, Microfluidics and Nanofluidics* 3, no. 1 (2016): 59–62.

46. P. Golub and M. Vasnetsov, "Photo-Alignment Control of Topological Defects in Nematic Liquid-Crystal Cells," *Ukrainian Journal of Physical Optics* 22, no. 2 (2021): 87–91.

47. N. Y. J. Tan, X. Zhang, D. W. K. Neo, R. Huang, K. Liu, and A. S. Kumar, "A Review of Recent Advances in Fabrication of Optical Fresnel Lenses," *Journal of Manufacturing Processes* 71 (2021): 113–133.

48. L. Lucchetti, L. Catani, and F. Simoni, "Light-Controlled Electric Freedericksz Threshold in Dye Doped Liquid Crystals," *Journal of Applied Physics* 115, no. 20 (2014): 203111.

49. E. Hecht, "Optics, 4th Editio Ed," *Addison-Wesley, San Francisco* 2 (2002): 3.

50. P. Yeh and C. Gu, *Optics of Liquid Crystal Displays* (Wiley, 1999).

51. A. D'Errico, F. Cardano, M. Maffei, et al., "Two-Dimensional Topological Quantum Walks in the Momentum Space of Structured Light," *Optica* 7, no. 2 (2020): 108–114.

52. A. Sit, F. Di Colandrea, A. D'Errico, and E. Karimi, "Spatially Twisted Liquid-Crystal Devices," *APL Photonics* 9, no. 5 (2024): 056112.

53. I. Rushnova, A. Murauski, V. Mikulich, and A. Muravsky, "High Anchoring Composite Photoalignment Material with High Photosensitivity," in *Proceedings of the 23rd International Display Workshops in Conjunction with Asia Display* (Curran Associates, 2016), LCT1–3.

54. A. A. Muravsky, A. A. Murauski, I. N. Kukhta, and A. S. Yakovleva, "High Anchoring Photoalignment Material Based on New Photo-Induced Hole Dipoles' Mechanism," *Journal of the Society for Information Display* 29, no. 11 (2021): 833–839.

55. A. Muravsky and A. Murauski, "40.3: Effect of Birefringent Alignment Layer on Azimuthal Anchoring Energy Measurement," in *SID Symposium Digest of Technical Papers*, vol. 52 (Wiley Online Library, 2021), 497–499.

56. A. Muravsky, V. Stanevich, D. Chepeleva, I. Kukhta, and A. Murauski, "81.2: New Concept of High Photosensitive Strong Anchoring Photoalignment," in International Conference on Display Technology (2025).

57. A. Murauski, S. Serdechnaya, and H.-S. Kwok, "P-132: Real-Time Simulation Software for Electro-Optical Calculation of LC Cells," in *SID Symposium Digest of Technical Papers*, vol. 38, no. 1 (Wiley Online Library, 2007), 702–705.

Supporting Information

Additional supporting information can be found online in the Supporting Information section.

Supporting File: lpor71391-sup-0001-SuppMat.pdf.